

Alternating absorption features during attosecond-pulse propagation in a laser-controlled gaseous medium

Adrian N. Pfeiffer,^{1,3,*} M. Justine Bell,^{1,3} Annelise R. Beck,^{1,3} Hiroki Mashiko,^{1,3}
Daniel M. Neumark,^{1,3} and Stephen R. Leone^{1,2,3}

¹*Department of Chemistry, University of California at Berkeley, Berkeley, California 94720, USA*

²*Department of Physics, University of California at Berkeley, Berkeley, California 94720, USA*

³*Ultrafast X-ray Science Laboratory, Chemical Sciences Division, Lawrence Berkeley National Laboratory, Berkeley, California 94720, USA*

(Received 28 August 2013; published 20 November 2013)

Recording the transmitted spectrum of a weak attosecond pulse through a medium, while a strong femtosecond pulse copropagates at variable delay, probes the strong-field dynamics of atoms, molecules, and solids. Usually, the interpretation of these measurements is based on the assumption of a thin medium. Here, the propagation through a macroscopic medium of helium atoms in the region of fully allowed resonances is investigated both theoretically and experimentally. The propagation has dramatic effects on the transient spectrum even at relatively low pressures (50 mbar) and short propagation lengths (1 mm). The absorption does not evolve monotonically with the product of propagation distance and pressure, but regions with characteristics of Lorentz line shapes and characteristics of Fano line shapes alternate. Criteria are deduced to estimate whether macroscopic effects can be neglected or not in a transient absorption experiment. Furthermore, the theory in the limit of single-atom response yields a general equation for Lorentz- and Fano-type line shapes at variable pulse delay.

DOI: [10.1103/PhysRevA.88.051402](https://doi.org/10.1103/PhysRevA.88.051402)

PACS number(s): 32.80.Qk, 42.50.Hz, 42.50.Gy

Time-resolved transient absorption spectroscopy is a rather new direction for attosecond physics [1]. Typically, the transient absorption of an attosecond pulse in the extreme ultraviolet (XUV) regime is measured while a strong femtosecond pulse in the near infrared (NIR) regime copropagates at variable pulse delay δt . In contrast to photoelectron measurements, where single atoms or molecules can be probed, absorption spectroscopy usually probes a macroscopic medium, because the attenuation by a single atom or molecule is vanishingly small. The effects of pulse propagation need to be understood in order to distinguish between single-atom effects and macroscopic effects.

Although the experimental setups are always similar, the scopes of the measurements are very diverse. One direction utilizes attosecond transient absorption to observe fast dynamics in atoms and molecules following some trigger event. When a strong-field ionizing NIR pulse is first, transient absorption can probe the electron movement in the valence shell of the ion [2]. When the XUV pulse is first, transient absorption can be used to determine the lifetime of excited states [3]. When the pulses overlap, the instantaneous Stark shift can be observed [4].

Another direction with transient absorption utilizes the combination of XUV and NIR pulses to achieve coherent optical control over the medium: the XUV (or x-ray) transparency is modified by a NIR dressing field [5–10]. Autler-Townes splitting into multiple branches has been observed on core-hole transitions [11,12]. Light-induced states have been observed [13,14]. Absorption can be manipulated on a subcycle time scale of the NIR field [14,15]. The laser control of Lorentz and Fano line shapes has been discovered [16–18].

Most of the experiments and theory rely on the assumption of a thin medium. Simulations including macroscopic propagation effects have been performed [17,19–24], but the reported computations are demanding and do not allow rapid estimates of propagation effects. More importantly, those simulations make use of a numerical integration in the time domain, which precludes making calculations involving states with lifetimes longer than a few picoseconds.

In this Rapid Communication, a systematic study of macroscopic propagation effects is presented on the example of the $1s^2-1s2p$ and $1s^2-1s3p$ transitions in helium. For the case that the XUV pulse is first, the reshaping of the absorption spectrum during the propagation does not evolve monotonically, but it exhibits ebb and flow stages. It is known from pulse propagation in coherent media (for example, pulse propagation in electromagnetically induced transparency) that a continuous control field can significantly alter the susceptibility of the medium [25]. Similarly here, in the case of a short-pulse control field, the absorption is not simply governed by the imaginary part of the susceptibility χ , as is the case if no NIR pulse is present and the Beer-Lambert law is valid. Instead the absorption features alternate in stages, where both the imaginary and the real part of χ influence the absorbance behavior.

The wave equation in one dimension describing the propagation of the pulse spectrum $\tilde{E}(\omega, x, \delta t)$ along the propagation direction x can be approximated by [23]

$$\frac{\partial}{\partial x} \tilde{E}(\omega, x, \delta t) = -i \frac{2\pi\omega}{c} \tilde{P}(\omega, x, \delta t) \quad (1)$$

(atomic units are used throughout this Rapid Communication). The atomic response to the attosecond and femtosecond pulses is described by the density matrix $\rho(t, x, \delta t)$, which is determined by the von Neumann equation with inclusion of

*Present address: Institute for Optics and Quantum Electronics, Friedrich Schiller University Jena, Max-Wien-Platz 1, 07743 Jena, Germany; a.n.pfeiffer@uni-jena.de

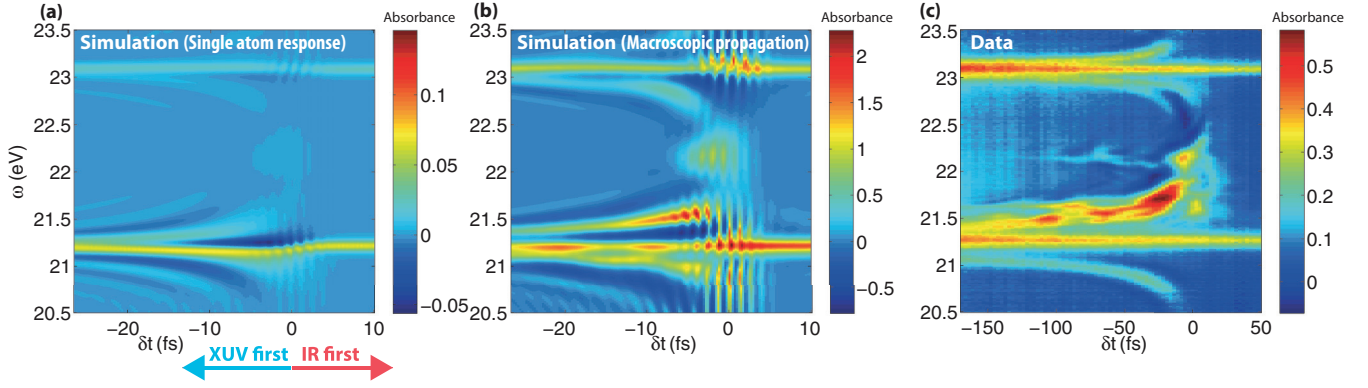


FIG. 1. (Color online) Transient absorption spectra. The absorbance is calculated at a pressure of 50 mbar with a propagation length $x = 2.5 \mu\text{m}$ (a) and $x = 1 \text{ mm}$ (b) based on Eqs. (1)–(3). Shorter propagation lengths do not change the transient absorption spectrum significantly; therefore (a) can be regarded as the single-atom response. The experimentally measured transient absorption spectrum is shown in (c).

decay rates,

$$i\dot{\rho}(t, x, \delta t) = [\mathcal{H}(t, x, \delta t), \rho(t, x, \delta t)] - i \frac{\gamma_{ij}}{2} \circ \rho(t, x, \delta t). \quad (2)$$

The Hamiltonian \mathcal{H} is defined as $\mathcal{H} = \mathcal{H}_0 - \mathbf{M}E(t, x, \delta t)$, where \mathcal{H}_0 is the unperturbed Hamiltonian and \mathbf{M} is the dipole matrix. The relation between the density matrix and the polarization $\tilde{P}(\omega, x, \delta t)$ is given by

$$P(t, x, \delta t) = N \text{Tr}[\rho(t, x, \delta t) \mathbf{M}], \quad (3)$$

where N is the atomic number density. The convention for the Fourier transformation is $\tilde{P}(\omega, x, \delta t) = (1/\sqrt{2\pi}) \int_{-\infty}^{\infty} P(t, x, \delta t) e^{-i\omega t} dt$. The elements of \mathbf{M} at indices (i, j) are termed and μ_{ij} in the following. The decay rate γ_{ij} of the polarization between states i and j is also the linewidth of the transition $i-j$. The dephasing time of the polarization is given by $T_{ij} = 2/\gamma_{ij}$ and is mainly given by the natural lifetime of the involved states for the present case.

Figures 1(a) and 1(b) show a numerical simulation based on Eqs. (1)–(3). A weak attosecond pulse (pulse duration: 500 as, center energy: 22.5 eV, peak intensity: 10^9 W/cm^2) at a variable delay δt and a strong femtosecond pulse (pulse duration: 5 fs, center wavelength: 780 nm, peak intensity: $2 \times 10^{12} \text{ W/cm}^2$) interact with a sample of gaseous helium at a pressure of 50 mbar. The following states are included ($1s^2, 1s2p, 1s3p, 1s2s, 1s3s, 1s4s, 1s5s, 1s3d, 1s4d, 1s5d$). Ionization to the continuum is neglected. The energies of the states and the dipole transitions are taken from [26]; γ_{ij} is assumed as 5 meV for $i \neq j$, 0 eV for $i = j = 0$ and 10 meV otherwise. The absorbance $A(\omega, x, \delta t)$ is calculated as

$$A(\omega, x, \delta t) = \ln[|\tilde{E}(\omega, 0, \delta t)|^2 / |\tilde{E}(\omega, x, \delta t)|^2]. \quad (4)$$

For the absorbance spectra shown in this Rapid Communication, the power spectra $|\tilde{E}(\omega, 0, \delta t)|^2$ and $|\tilde{E}(\omega, x, \delta t)|^2$ are first convoluted with an instrumental linewidth of 40 meV (FWHM) before the absorbance is calculated to mimic the spectral resolution in an experiment. This convolution is important for a quantitative comparison of data and simulation, but it does not influence the qualitative features of the absorbance spectra.

The experimental results shown in Fig. 1(c) are obtained as described in Ref. [13], except that the pressure in the gas cell was significantly increased. The pressure is estimated as 50 mbar, but the variability of the laser beam holes in the gas cell makes the estimate imprecise over the range of 10–240 mbar. The parameters of the femtosecond pulse [pulse duration: 12 fs, center wavelength: 780 nm, peak intensity: $(4 \pm 2) \times 10^{12} \text{ W/cm}^2$] are similar to the parameters used in the simulation.

The transient absorption spectrum in the limit of a thin medium [Fig. 1(a)] looks substantially different from the spectrum after the propagation through 1 mm of the medium [Fig. 1(b)]. The absorption feature around 22.2 eV that appears in the region of pulse overlap (this absorption feature has been interpreted as belonging to a light-induced state [13]) is enhanced. For negative pulse delays (where the XUV pulse is first), the absorption line belonging to the $1s^2-1s2p$ transition at 21.2 eV is split into three distinct lines with complex intensity variations after the propagation. These observations are already a first hint that the absorption does not scale linearly with the product of pressure and propagation length, but rather that it evolves nonlinearly. The shape of the experimentally measured transient absorption trace [Fig. 1(c)] agrees qualitatively well with the simulation after propagation [Fig. 1(b)], but it is to be noted that the time axes are very different.

In order to understand the effects that occur during the propagation, the problem is treated in a simplified model (Fig. 2). It is assumed that the XUV pulse arrives first. The time axis is separated into three domains. Domain I denotes the time before the NIR pulse is on. Here, only the ground state and one excited state (the state $1s2p$ in the following example) are considered. In the limit of negligible population transfer (perturbative approximation) and $\gamma_{12}^2 \ll \omega_{12}^2$, Eqs. (2) and (3) can be converted into

$$\begin{aligned} \ddot{P}(t, x, \delta t) + \gamma_{12} \dot{P}(t, x, \delta t) + \omega_{12}^2 P(t, x, \delta t) \\ = 2N\omega_{12}\mu_{12}^2 E(t, x, \delta t), \end{aligned} \quad (5)$$

where ω_{12} is the energy difference of the two states. For the present example, $\omega_{12} = 21.2 \text{ eV}$, $\gamma_{12} = 5 \text{ meV}$, and $\mu_{12} = 0.42$. Domain II denotes the time when the NIR pulse is on.

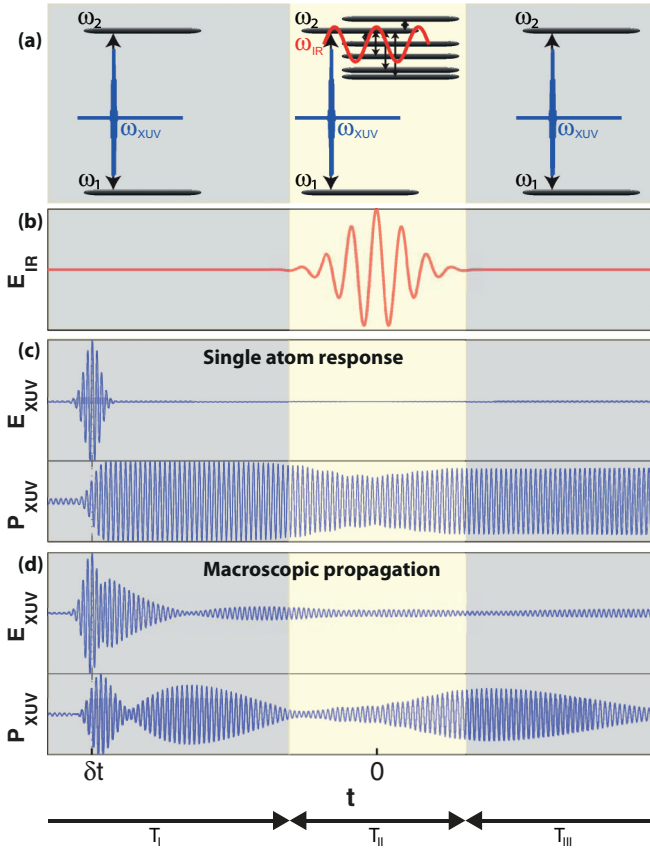


FIG. 2. (Color online) Time-domain picture of absorption. (a) Contributing states in time domains I–III. (b) NIR pulse. (c) The XUV pulse triggers the polarization response P_{XUV} . A strong NIR pulse follows at $t = 0$ and disturbs the evolving polarization P_{XUV} , an effect that persists beyond the NIR pulse duration. (d) After propagation, a tail follows the attosecond pulse according to Eq. (1). In the spectral domain, this tail appears as an absorption line, because the oscillations in this tail are out of phase with regard to the leading attosecond pulse. The tail appears also if no NIR pulse is present, but the NIR pulse disturbs the tail for $t > 0$.

Additional levels have to be considered for strong-field coupling, and further strong-field effects such as strong-field ionization and Stark shift of the energy levels occur. Domain III denotes the time after the NIR pulse is on and is treated as domain I.

In the limit of a short NIR pulse ($T_{II} \rightarrow 0$, where T_{II} is the time span of domain II) and in the vicinity of the resonance ($|\omega - \omega_{12}| \ll \omega$), an expression for the frequency-dependent polarization can be derived:

$$\tilde{P}(\omega, x, \delta t) = \chi \tilde{E}(\omega, x, \delta t) + i\chi \frac{(L-1)Q(\delta t)}{\sqrt{8\pi} N \mu_{12}^2} \quad (6)$$

where the parameters χ , L , and $Q(\delta t)$ are defined further below. Equation (6) is the main result of this Rapid Communication. It allows the convenient and fast calculation of the spectral reshaping during macroscopic propagation, where the values for the dephasing times are not limited to a few picoseconds as for the integration of Eq. (2).

The susceptibility χ is approximated by

$$\chi = \frac{2N\omega_{12}\mu_{12}^2}{\omega_{12}^2 - \omega^2 + i\gamma_{12}\omega}. \quad (7)$$

The parameter L is a complex number with $|L| < 1$ that describes the amplitude and phase change that the NIR pulse induces in $P(t)$ and is defined as

$$L = \int_{t_3}^{\infty} P(t)e^{-i\omega_{12}t} dt / \int_{t_3}^{\infty} P_{\text{ref}}(t)e^{-i\omega_{12}t} dt, \quad (8)$$

where $P_{\text{ref}}(t)$ is the reference polarization where the intensity of the NIR pulse is set to zero and t_3 is the beginning of time domain III. L can be calculated numerically with the use of Eqs. (3) and (8). In the present case, L is estimated as $L = 0.9\exp(-i2.2)$. If the calculated absorbance spectra are to be compared with data, then L can be estimated by curve fitting.

The parameter $Q(\delta t)$ is defined as

$$Q(\delta t) = \frac{2}{\sqrt{2\pi}} \int_0^{\infty} \chi \tilde{E}(\omega, x=0, \delta t) e^{-i\frac{2\pi\omega}{c}\chi x} d\omega, \quad (9)$$

and can be interpreted as the strength of the time-dependent polarization at the time of the NIR pulse. In the case of an infinitely short attosecond pulse, $\tilde{E}(\omega, x=0, \delta t) = E_0 e^{-i\omega\delta t}$, $Q(\delta t)$ reduces to

$$Q(\delta t) = \frac{2}{\sqrt{2\pi}} E_0 \int_0^{\infty} \chi e^{-i(\frac{2\pi}{c}\chi x + \delta t)\omega} d\omega. \quad (10)$$

Introducing the parameter $p_1 = |\chi|\omega x/c$ reveals a criterion for propagation that will be important: Propagation effects can be neglected for $p_1 \ll 1$ (<0.01 is very safe) and can become important when p_1 is on the order of 1. In the present example, p_1 reaches the value 40 after the full propagation length of 1 mm, and the value 1 is reached after a propagation length of 25 μm .

The parameter p_1 is very sensitive to the linewidth γ_{12} , such that longer dephasing times increase the propagation effects. This is the reason why the simulation in Fig. 1(b) deviates from the data in the values of the pulse delay: The linewidth γ_{12} was assumed as 5 meV in the simulation for the feasibility of the computation, corresponding to a dephasing time of 263 fs, but the real dephasing time is on the order of a nanosecond [27].

Figure 3 shows a comparison of a full simulation based on Eqs. (1)–(3) and the analytical approximation using Eq. (6). The essential features of macroscopic propagation are captured in the analytical approximation. Close to the overlap of the XUV and NIR pulses, the approximation deviates.

Figure 4 shows the propagation at a fixed pulse delay of -30 and -5 fs. Various interesting reshaping effects are observed. Absorption lines can split and shift in energy during the propagation. Even more surprisingly, the absorption lines do not evolve monotonically, but they can ebb and flow repeatedly. The parameter $Q(\delta t)$, also plotted in Fig. 4, signals where ebb and flow alternates. The interpretation for this rich dynamic behavior can be deduced from Eq. (6): Absorption without the presence of an NIR pulse follows the imaginary part of the susceptibility χ . This leads to Lorentz line shapes. In the presence of a delayed NIR pulse, the real part of the susceptibility χ (which has the characteristic

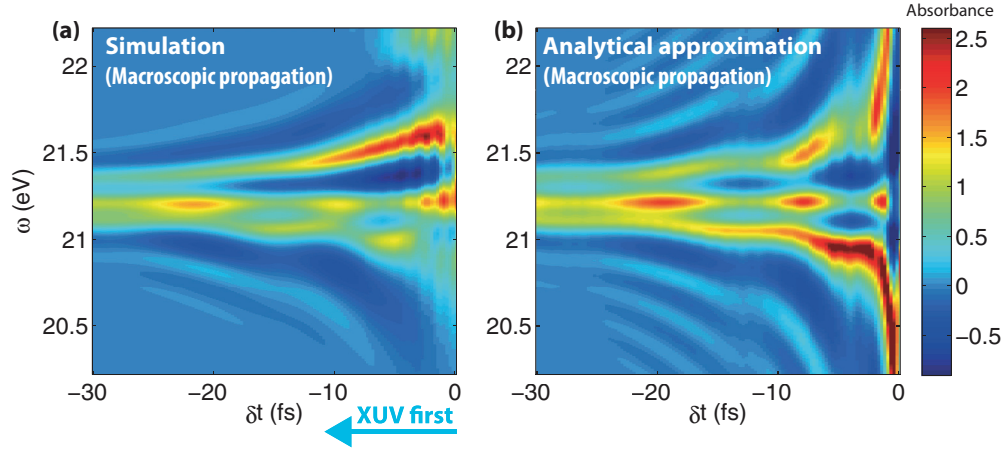


FIG. 3. (Color online) Comparison of numerical simulation and analytical approximation. The transient absorption spectra for the $1s^2-1s2p$ transition are numerically simulated (a) based on Eqs. (1) and (3) and analytically calculated (b) with Eq. (6). The propagation is calculated at a pressure of 50 mbar with a propagation length $x = 1$ mm.

Fano line shape) also affects the absorption. Depending on the complex value of $(L-1)Q(\delta t)$ in Eq. (6), the action of the NIR pulse induces Lorentz or Fano profiles, and leads to absorption or emission. With $Q(\delta t)$ alternating its value during the propagation, regions in the medium with Lorentz characteristics and regions with Fano characteristics alternate as the XUV pulse propagates through the medium.

For the limiting case of a thin medium ($x = 0$), $Q(\delta t)$ can be calculated and Eq. (6) reduces to

$$\tilde{P}(\omega, x = 0, \delta t) = \chi \tilde{E}(\omega, x = 0, \delta t) \left[1 + e^{i(\omega - \omega_{12})\delta t} (L - 1) e^{\frac{\gamma_{12}}{2}\delta t} \right]. \quad (11)$$

Equation (11) is a generalization of the laser-controlled Lorentz- and Fano-type line shapes discovered in Ref. [16]. For zero pulse delay ($\delta t = 0$), Eq. (11) can be transformed into Eq. (6) of Ref. [16] if the single-atom response function ($A(\omega) \propto \text{Im}\{\tilde{E}^*(\omega)\tilde{P}(\omega)\}$; see Ref. [19]) is used. For the case that the XUV pulse is first, additional absorption lines appear that follow a hyperbolic curve as a function of pulse delay (Fig. 5). This is an analogy to spatial diffraction: When a plane wave passes through an aperture, then a diffraction pattern with side peaks appears in the far field. Here, an aperture is formed by the attosecond pulse that starts the polarization and the NIR pulse that alters the polarization. The smaller the aperture (the

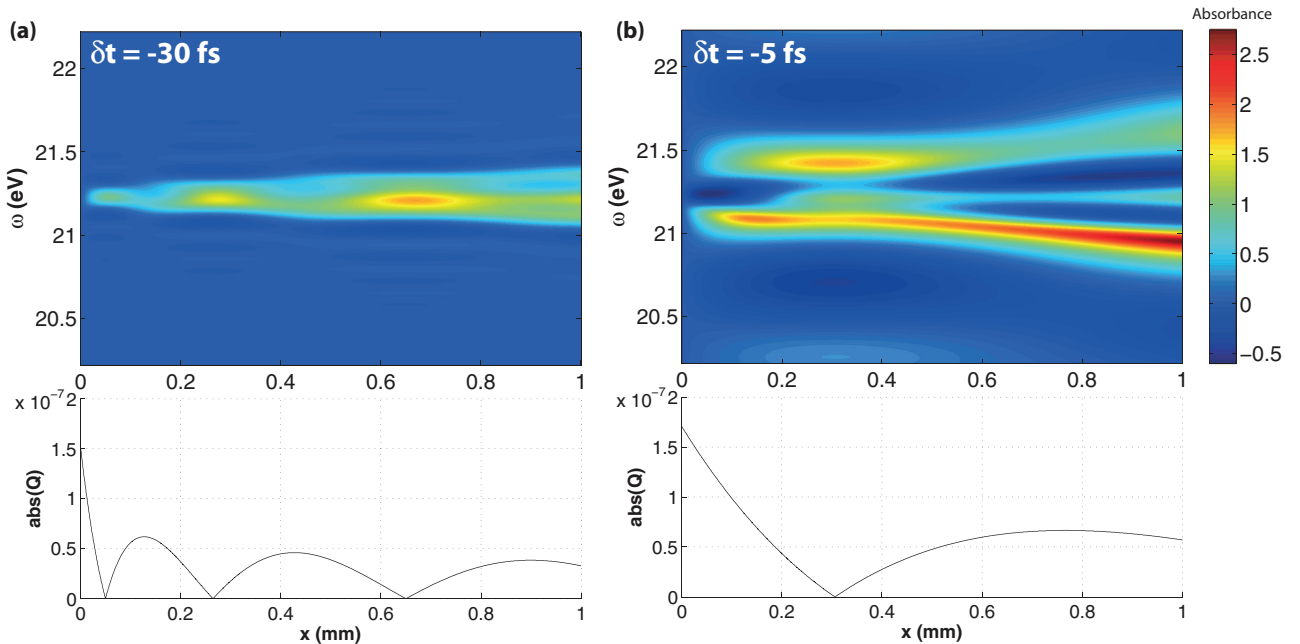


FIG. 4. (Color online) Spectral reshaping during propagation. The absorption profile of the $1s^2-1s2p$ transition as a function of the propagation length x at a fixed pump-probe delay $\delta t = -30$ fs (a) and $\delta t = -5$ fs (b). The calculation is done with Eq. (6), but the full simulation based on Eqs. (2) and (3) leads to very similar spectra. The absolute value of the parameter $Q(\delta t)$ [Eq. (10)] is shown in the lower panels.

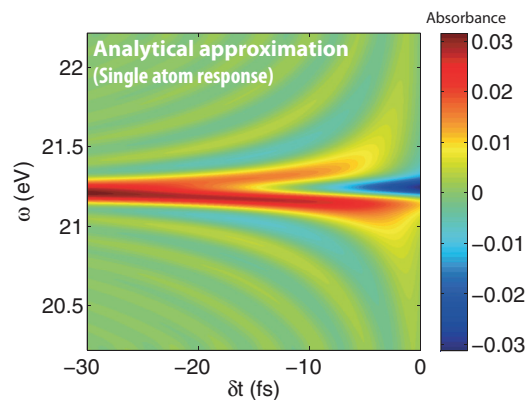


FIG. 5. (Color online) Single-atom response. The transient absorption spectrum for the $1s^2-1s2p$ transition is calculated with Eq. (11) for $L = 0.9\exp(-i2.2)$. The propagation is calculated at a pressure of 50 mbar with a propagation length $x = 1 \mu\text{m}$. Shorter propagation lengths do not change the transient absorption spectrum significantly; therefore this spectrum shows the single-atom response.

smaller the pulse delay), the bigger is the separation of the side peaks.

Introducing a parameter $p_2 = \exp(\gamma_{12}\delta t/2)$ reveals another criterion: Propagation effects can be neglected for $p_2 \ll 1$ and can become important when p_2 is on the order of 1. The interpretation is that the NIR pulse does not alter the XUV polarization when the pulse delay is long compared to the dephasing time of the states.

According to Eq. (11), the transient absorption trace on resonance ($\omega = \omega_{12}$) evolves as $\exp(\gamma_{12}\delta t/2)$. This has been

used to determine the lifetime of autoionizing states of argon [3], but the method is limited to cases where the spectrometer resolution is much better than the linewidth. With Eq. (11), the transient absorption can be determined as a function of δt and ω , such that the absorbance can be calculated after convolution with the spectrometer resolution and be fitted to the data.

In conclusion, an equation is derived for the convenient calculation of propagation effects in transient absorption measurements. Surprisingly, the absorption does not evolve monotonically as the pulse propagates in the medium. The reason is that stages alternate in the medium where the imaginary part or the real part of the susceptibility χ dominates, corresponding to Lorentz and Fano line shapes, respectively. Parameters p_1 and p_2 assess the severity of macroscopic effects. For the case of a thin medium, an analytical equation is derived for laser-controlled line shapes at variable pulse delay. This allows the determination of lifetimes from transient absorption traces and can be used to extract details of strong-field processes in excited states.

A.N.P. is supported by the Laboratory Directed Research and Development Program at Lawrence Berkeley National Laboratory, and the experimental work is supported by the Ultrafast X-Ray Laser Science Program at Lawrence Berkeley National Laboratory, the Director, Office of Science, Office of Basic Energy Sciences, of the US Department of Energy under Contract No. DE-AC03-76SF00098. S.R.L. acknowledges support from the Office of Assistant Secretary of Defense for Research and Engineering, National Security Science and Engineering Faculty Fellowship.

- [1] F. Krausz and M. Ivanov, *Rev. Mod. Phys.* **81**, 163 (2009).
- [2] E. Goulielmakis, Z. H. Loh, A. Wirth, R. Santra, N. Rohringer, V. S. Yakovlev, S. Zherebtsov, T. Pfeifer, A. M. Azzeer, M. F. Kling, S. R. Leone, and F. Krausz, *Nature* **466**, 739 (2010).
- [3] H. Wang, M. Chini, S. Chen, C. H. Zhang, Y. Cheng, F. He, Y. Wu, U. Thumm, and Z. Chang, *Phys. Rev. Lett.* **105**, 143002 (2010).
- [4] M. Chini, B. Z. Zhao, H. Wang, Y. Cheng, S. X. Hu, and Z. H. Chang, *Phys. Rev. Lett.* **109**, 073601 (2012).
- [5] C. Buth, R. Santra, and L. Young, *Phys. Rev. Lett.* **98**, 253001 (2007).
- [6] T. E. Glover, M. P. Hertlein, S. H. Southworth, T. K. Allison, J. van Tilborg, E. P. Kanter, B. Krässig, H. R. Varma, B. Rude, R. Santra, A. Belkacem, and L. Young, *Nat. Phys.* **6**, 69 (2010).
- [7] P. Ranitovic, X. M. Tong, C. W. Hogle, X. Zhou, Y. Liu, N. Toshima, M. M. Murnane, and H. C. Kapteyn, *Phys. Rev. Lett.* **106**, 193008 (2011).
- [8] M. Tarana and C. H. Greene, *Phys. Rev. A* **85**, 013411 (2012).
- [9] Z. H. Loh, C. H. Greene, and S. R. Leone, *Chem. Phys.* **350**, 7 (2008).
- [10] J. Herrmann, M. Weger, R. Locher, M. Sabbar, P. Rivière, U. Saalman, J.-M. Rost, L. Gallmann, and U. Keller, *Phys. Rev. A* **88**, 043843 (2013).
- [11] M.-F. Lin, A. N. Pfeiffer, D. M. Neumark, O. Gessner, and S. R. Leone, *J. Chem. Phys.* **137**, 244305 (2012).
- [12] A. N. Pfeiffer and S. R. Leone, *Phys. Rev. A* **85**, 053422 (2012).
- [13] S. H. Chen, M. J. Bell, A. R. Beck, H. Mashiko, M. Wu, A. N. Pfeiffer, M. B. Gaarde, D. M. Neumark, S. R. Leone, and K. J. Schafer, *Phys. Rev. A* **86**, 063408 (2012).
- [14] M. Chini, X. Wang, Y. Cheng, Y. Wu, D. Zhao, D. A. Telnov, S.-I. Chu, and Z. Chang, *Sci. Rep.* **3**, 1105 (2013).
- [15] S. Chen, M. Wu, M. B. Gaarde, and K. J. Schafer, *Phys. Rev. A* **87**, 033408 (2013).
- [16] C. Ott, A. Kaldun, P. Raith, K. Meyer, M. Laux, J. Evers, C. H. Keitel, C. H. Greene, and T. Pfeifer, *Science* **340**, 716 (2013).
- [17] W.-C. Chu and C. D. Lin, *Phys. Rev. A* **87**, 013415 (2013).
- [18] J. Zhao and M. Lein, *New J. Phys.* **14**, 065003 (2012).
- [19] M. B. Gaarde, C. Buth, J. L. Tate, and K. J. Schafer, *Phys. Rev. A* **83**, 013419 (2011).
- [20] S. Chen, K. J. Schafer, and M. B. Gaarde, *Opt. Lett.* **37**, 2211 (2012).
- [21] W.-C. Chu and C. D. Lin, *J. Phys. B* **45**, 201002 (2012).
- [22] M. Wu, S. Chen, K. J. Schafer, and M. B. Gaarde, *Phys. Rev. A* **87**, 013828 (2013).
- [23] R. Santra, V. S. Yakovlev, T. Pfeifer, and Z. H. Loh, *Phys. Rev. A* **83**, 033405 (2011).
- [24] S. Chen, M. Wu, M. B. Gaarde, and K. J. Schafer, *Phys. Rev. A* **88**, 033409 (2013).
- [25] M. Fleischhauer, A. Imamoglu, and J. P. Marangos, *Rev. Mod. Phys.* **77**, 633 (2005).
- [26] NIST Atomic Spectra Database, <http://physics.nist.gov/asd>.
- [27] S. Heron, R. W. P. McWhirter, and E. H. Roderick, *Proc. R. Soc. London, Ser. A* **234**, 565 (1956).